Since January 2020 Elsevier has created a COVID-19 resource centre with free information in English and Mandarin on the novel coronavirus COVID-19. The COVID-19 resource centre is hosted on Elsevier Connect, the company's public news and information website.

Antiviral Research 150 (2018) 155–163

Contents lists available at ScienceDirect

Antiviral Research

journal homepage: www.elsevier.com/locate/antiviral

Disulfiram can inhibit MERS and SARS coronavirus papain-like proteases via different modes

Min-Han Lin[a], David C. Moses[b], Chih-Hua Hsieh[a], Shu-Chun Cheng[c], Yau-Hung Chen[b], Chiao-Yin Sun[c,**], Chi-Yuan Chou[a,*]

[a] Department of Life Sciences and Institute of Genome Sciences, National Yang-Ming University, Taipei 112, Taiwan
[b] Department of Chemistry, Tamkang University, Tamsui 251, Taiwan
[c] Department of Nephrology, Chang-Gung Memorial Hospital, Keelung 204, Taiwan

ARTICLE INFO

Keywords:
MERS- and SARS-CoV
Papain-like protease
Disulfiram
6-Thioguanine
Mycophenolic acid
Synergistic inhibition

ABSTRACT

Severe acute respiratory syndrome coronavirus (SARS-CoV) emerged in southern China in late 2002 and caused a global outbreak with a fatality rate around 10% in 2003. Ten years later, a second highly pathogenic human CoV, MERS-CoV, emerged in the Middle East and has spread to other countries in Europe, North Africa, North America and Asia. As of November 2017, MERS-CoV had infected at least 2102 people with a fatality rate of about 35% globally, and hence there is an urgent need to identify antiviral drugs that are active against MERS-CoV. Here we show that a clinically available alcohol-aversive drug, disulfiram, can inhibit the papain-like proteases (PL^{pro}s) of MERS-CoV and SARS-CoV. Our findings suggest that disulfiram acts as an allosteric inhibitor of MERS-CoV PL^{pro} but as a competitive (or mixed) inhibitor of SARS-CoV PL^{pro}. The phenomenon of slow-binding inhibition and the irrecoverability of enzyme activity after removing unbound disulfiram indicate covalent inactivation of SARS-CoV PL^{pro} by disulfiram, while synergistic inhibition of MERS-CoV PL^{pro} by disulfiram and 6-thioguanine or mycophenolic acid implies the potential for combination treatments using these three clinically available drugs.

1. Introduction

Before 2002, human coronaviruses (CoVs) had the reputation of occasionally emerging from zoonotic sources and causing mild respiratory tract infections. In late 2002, however, without any warning, severe acute respiratory syndrome (SARS) emerged and spread by coronaviral infection to become a pandemic, mainly in Asia but also in other regions, with a fatality rate of 10% (Hilgenfeld and Peiris, 2013). Ten years later, when SARS had almost been forgotten, a second highly pathogenic human CoV, MERS, caused the severe respiratory syndrome in the Middle East and then spreading to other countries due to human activity (Zaki et al., 2012). MERS-CoV has infected at least 2100 people with a high mortality rate of 35% since 2012 (http://www.who.int/csr/don/7-november-2017-mers-saudi-arabia/en/). Because of international travel and climate change, we cannot rule out the possibility of the emergence of additional highly pathogenic CoVs in the near future (Menachery et al., 2015, 2016). Thus, the development of antiviral drugs effective against CoVs is urgently needed.

CoVs are positive-sense single-stranded RNA viruses. After the virion has entered the host cell, two polyproteins, pp1a and pp1ab, are directly translated and then cleaved by two viral proteases, main protease (M^{pro}) and papain-like protease (PL^{pro}) (Perlman and Netland, 2009). PL^{pro} is responsible for the cleavage of non-structural proteins (nsp) 1, 2 and 3 while M^{pro} cleaves all junctions downstream of nsp4 (Perlman and Netland, 2009). In addition, PL^{pro} can deubiquitinate or deISGylate host cell proteins, including interferon factor 3 (IRF3), and inactivate the pathway of nuclear factor κ-light-chain-enhancer of activated B cells (NF-κB), resulting in the immune suppression of host cells (Clementz et al., 2010; Frieman et al., 2009; Yang et al., 2014; Zheng et al., 2008). Due to its multiple roles in viral replication and host cell control, PL^{pro} is considered a potential antiviral target.

Disulfiram is a drug which has been approved by the United States Food and Drug Administration (FDA) for use in alcohol aversion therapy since 1951 (Bell and Smith, 1949; Krampe and Ehrenreich, 2010; Moore et al., 1998). It is known to irreversibly inhibit hepatic aldehyde dehydrogenase (Lipsky et al., 2001). Recent studies indicate

Abbreviations: CoV, coronavirus; M^{pro}, main protease; DDC, diethyldithiolcarbamate; DUB, deubiquitination; MERS, Middle East respiratory syndrome; βME, β-mercaptoethanol; MPA, mycophenolic acid; NEM, N-ethylmaleimide; nsp, non-structural protein; PL^{pro}, papain-like protease; SARS, severe acute respiratory syndrome

* Corresponding author. 155 Li-Nong St., Sec. 2, Taipei 112, Taiwan.
** Corresponding author. 222 Mai-Chin Rd., Keelung 204, Taiwan.
E-mail addresses: fish3970@gmail.com (C.-Y. Sun), cychou@ym.edu.tw (C.-Y. Chou).

https://doi.org/10.1016/j.antiviral.2017.12.015
Received 31 August 2017; Received in revised form 11 November 2017; Accepted 20 December 2017
Available online 28 December 2017

that disulfiram is able to inhibit other enzymes, such as methyltransferase, urease and kinase, all by reacting with important cysteine residues, suggesting broad-spectrum characteristics (Diaz-Sanchez et al., 2016; Galkin et al., 2014; Paranjpe et al., 2014). In addition, there has been a clinical trial investigating the usage of disulfiram for reactivating latent HIV in order to make it accessible to highly active anti-retroviral therapy (Elliott et al., 2015), and the drug has also been shown to act as a "zinc ejector" with respect to hepatitis C virus NS5A protein (Lee et al., 2016). However, the effect of disulfiram on viral cysteine proteases is still unknown. In the present study, we demonstrate that disulfiram is an inhibitor of MERS-CoV and SARS-CoV PL^{pro}s, and furthermore that disulfiram acts on MERS-CoV and SARS-CoV PL^{pro} via different inhibition mechanisms. Moreover, we investigated the synergies between a number of known PL^{pro} inhibitors and disulfiram, and our results point to the possibility of using combination treatments involving disulfiram and other clinically available drugs against CoVs.

2. Materials and methods

2.1. Recombinant protein production

The SARS-CoV PL^{pro} C271A mutation was introduced using the QuikChange mutagenesis kit (Stratagene) and was verified by DNA sequencing. The forward primer was 5′-gtacactggtaactatcaggcgggtcatt acactcatata and the reverse primer was 5′-tatatgagtgtaatgacccgcctgatagttaccagtgtac. The MERS-CoV and SARS-CoV PL^{pro}s and the SARS-CoV PL^{pro} C271A mutant protein were produced and purified as previously described (Chou et al., 2012, 2014; Lin et al., 2014). Briefly, the cultures were grown at 37 °C for 4 h, then induced with 0.4 mM isopropyl β-D-1-thiogalactopyranoside and grown at 20 °C for 20 h. The cell pellet was resuspended in lysis buffer (20 mM Tris, pH 8.5, 250 mM NaCl, 5% glycerol, 0.2% Triton X-100, 2 mM β-mercaptoethanol (βME)), lysed by sonication and then centrifuged to remove the insoluble pellet. The target protein was purified from the fraction of soluble proteins via nickel affinity chromatography, then loaded onto an S-100 gel-filtration column (GE Healthcare) equilibrated with running buffer (20 mM Tris, pH 8.5, 100 mM NaCl, 2 mM dithiothreitol). For the crystallization of SARS-CoV PL^{pro} in complex with glycerol, the reductant was removed and 50 μM disulfiram was added to each buffer during the purification process. The purity of the fractions collected was analyzed by SDS-PAGE and the protein was concentrated to 30 mg/ml using an Amicon Ultra-4 30-kDa centrifugal filter (Millipore).

2.2. Deubiquitination (DUB) assay

The DUB assay was carried out as previously described (Cheng et al., 2015; Chou et al., 2008; Lin et al., 2014). The fluorogenic substrate Ub-7-amino-4-trifluoro-methylcoumarin (Ub-AFC) (Boston Biochem) was added at a concentration of 0.25 μM along with various concentrations of inhibitors into 20 mM phosphate (pH 6.5) and each mixture was incubated at 30 °C for 3 min. After adding 0.2 μM coronaviral PL^{pro}, enzymatic activity was determined by continuously monitoring fluorescence intensity at excitation and emission wavelengths of 350 and 485 nm, respectively. The data was fitted to obtain IC_{50} according to Eq. (1):

$$v = v_0/(1 + IC_{50}^n/[I]^n) \quad (1)$$

in which v is the initial velocity in the presence of inhibitor at concentration $[I]$ and v_0 is the initial velocity in the absence of inhibitor, while n is the Hill constant.

In addition, to test for the recoverability of activity, coronaviral PL^{pro} was incubated with or without 200 μM disulfiram for 1 h and then desalted using a Sephadex G-25 column. The DUB activity of 0.2 μM treated enzyme was then determined in the presence or absence of 5 mM βME.

2.3. Steady-state kinetic analysis

The peptidyl substrate Dabcyl-FRLKGGAPIKGV-Edans was used to measure the proteolytic activity of PL^{pro}. Fluorescence intensity was monitored at 329 nm (excitation) and 520 nm (emission) and converted to the amount of hydrolyzed substrate based on previous studies (Cheng et al., 2015; Chou et al., 2008). For inhibition studies, the reaction mixture contained 9–80 μM peptide substrate with 0–200 μM disulfiram in 20 mM phosphate (pH 6.5). MERS-CoV PL^{pro} at 0.6 μM and wild-type SARS-CoV PL^{pro} and C271A mutant at 0.05 μM was used, respectively. After adding the enzyme to the reaction mixture, fluorescence intensity was continuously monitored at 30 °C. The increase in fluorescence was linear for at least 1 min, and thus the slope of the line represented the initial reaction velocity (v).

The data obtained for the inhibition of MERS-CoV PL^{pro} by disulfiram was found to best fit a noncompetitive inhibition pattern in accordance with Eq. (2):

$$v = k_{cat}[E][S]/((1 + [I]/K_{is})(K_M + [S])) \quad (2)$$

while the data obtained for the inhibition of SARS-CoV PL^{pro} by disulfiram was found to best fit a competitive inhibition pattern in accordance with Eq. (3) or a mixed inhibition pattern in accordance with Eq. (4):

$$v = k_{cat}[E][S]/((1 + [I]/K_{is})K_M + [S]) \quad (3)$$

$$v = k_{cat}[E][S]/((1 + [I]/K_{is})K_M + (1 + [I]/\alpha K_{is})[S]) \quad (4)$$

in which k_{cat} is the rate constant, $[E]$, $[S]$ and $[I]$ denote the enzyme, substrate and inhibitor concentrations, and K_M is the Michaelis-Menten constant for the interaction between the peptide substrate and the enzyme. K_{is} is the slope inhibition constant for the enzyme-inhibitor complex and αK_{is} is the slope inhibition constant for the enzyme-substrate-inhibitor complex. The program SigmaPlot 12.5 (Systat Software Inc., USA) was used for data analysis.

2.4. Multiple inhibition assay

To characterize the mutual effects of disulfiram and other known PL^{pro} inhibitors, the activity of MERS-CoV PL^{pro} was measured with and without either 6-thioguanine (6TG) (0 and 15 μM) or mycophenolic acid (MPA) (0 and 150 μM) in the presence of various concentrations of disulfiram (0–30 μM), and that of SARS-CoV PL^{pro} was measured with and without either 6TG or N-ethylmaleimide (NEM) in the presence of various concentrations of disulfiram (0–24 μM). The concentrations of the peptidyl substrate and MERS-CoV PL^{pro} were 20 and 0.6 μM, respectively, while those of the substrate and SARS-CoV PL^{pro} were 15 and 0.05 μM, respectively. Data obtained from the reactions were fitted to Eq. (5):

$$v = v_0/(1 + [I]/K_i + [J]/K_j + [I][J]/\alpha K_i K_j) \quad (5)$$

where v is the initial velocity in the presence of both inhibitors, $[I]$ and $[J]$ are the concentrations of the two inhibitors, v_0 is the velocity in the absence of inhibitors, K_i and K_j are the apparent dissociation constants for the two inhibitors, and α is a measurement of the degree of interaction between the two inhibitors (Copeland, 2000; Yonetani and Theorell, 1964).

2.5. Zinc ejection assays

Release of zinc ions from coronaviral PL^{pro}s was monitored as the increase in fluorescence emission from the zinc-specific fluorophore FluoZin-3 (Thermo Fisher Scientific) (Lee et al., 2016). Briefly, the protein and FluoZin-3 were mixed in 20 mM phosphate buffer (pH 6.5) to concentrations of 5 μM and 1 μM, respectively, in the presence or absence of 5 μM disulfiram. Fluorescence emission was continuously measured at 25 °C using emission and excitation wavelengths of 494 nm

and 516 nm, respectively, in a PerkinElmer LS50B luminescence spectrometer.

2.6. Thermostability assays

The change in secondary structure of coronaviral PL^{pro}s in the absence and presence of 5 μM disulfiram was continuously measured using ellipticity at 222 nm as the temperature was ramped from 30 to 85 °C in a JASCO J-810 spectropolarimeter. The protein at 5 μM was dissolved into 20 mM phosphate buffer, pH 6.5. The width of the cuvette was 1 mm.

2.7. Inactivation mechanism

For the inactivation studies, SARS-CoV PL^{pro} (0.05 μM in 20 mM phosphate buffer, pH 6.5) was incubated with different concentrations of disulfiram and peptide substrate, and enzymatic activity was traced for 5 min. All progress curves recorded showed an exponential course and were analyzed according to the following integrated rate equation (Eq. (6)) (Copeland, 2000):

$$[P] = v_s t + [(v_i + v_s)/k_{inact}]\,[1 - \exp(-k_{inact}t)] + d \quad (6)$$

in which v_i is the initial velocity, v_s is the steady-state velocity, and d is the displacement on the y-axis. The replot of k_{inact} versus the concentration of disulfiram was fitted to a saturation curve according to Eq. (7) (Copeland, 2000):

$$k_{inact} = k_{max}[I]/(K_{inact} + [I]) \quad (7)$$

in which K_{inact} is the dissociation constant of the enzyme-disulfiram complex and k_{max} is the maximum inactivation rate constant.

2.8. Protein crystallization

Crystals of SARS-CoV PL^{pro} in complex with βME or glycerol were obtained at 22 °C by the sitting-drop vapor-diffusion method. For the PL^{pro}-βME complex, the protein at 15 mg/ml was incubated with 0.4 mM disulfiram for 1 h and then crystallized. Single crystals were grown in reservoir solution containing 16% (w/v) PEG 3350 and 0.1 M Bis-Tris propane (pH 8.0). For the PL^{pro}-glycerol complex, protein purified with the addition of 50 μM disulfiram into each buffer during the purification process was crystallized at 12.5 mg/ml. Single crystals were grown in reservoir solution containing 6% (w/v) PEG 8000 and 0.1 M HEPES (pH 8.0). All crystals were cryoprotected in reservoir solution supplemented with 15% and 25% (v/v) glycerol for PL^{pro}-βME and PL^{pro}-glycerol, respectively, and then flash-cooled in liquid nitrogen.

2.9. Data collection and structure determination

X-ray diffraction data was collected at 100 K on the SPXF beamline 15A1 at the National Synchrotron Radiation Research Center, Taiwan, ROC using a Rayonix MX300HE CCD detector at a wavelength of 1 Å. The diffraction images were processed and then scaled with the HKL-2000 package (Otwinowski and Minor, 1997). The structure was solved by the molecular-replacement method with Phaser (McCoy et al., 2007) using the structure of wild-type SARS-CoV PL^{pro} (PDB entry 2fe8; (Ratia et al., 2006)) as the search model. Manual rebuilding of the structure model was performed with Coot (Emsley and Cowtan, 2004). Structure refinement was carried out with REFMAC (Murshudov et al., 2011). Data-processing and refinement statistics are summarized in Table 3. The crystal structures of the SARS-CoV PL^{pro}-βME complex and SARS-CoV PL^{pro}-glycerol complex have been deposited in the Protein Data Bank (PDB entries 5y3q and 5y3e for PL^{pro}-βME and PL^{pro}-glycerol, respectively).

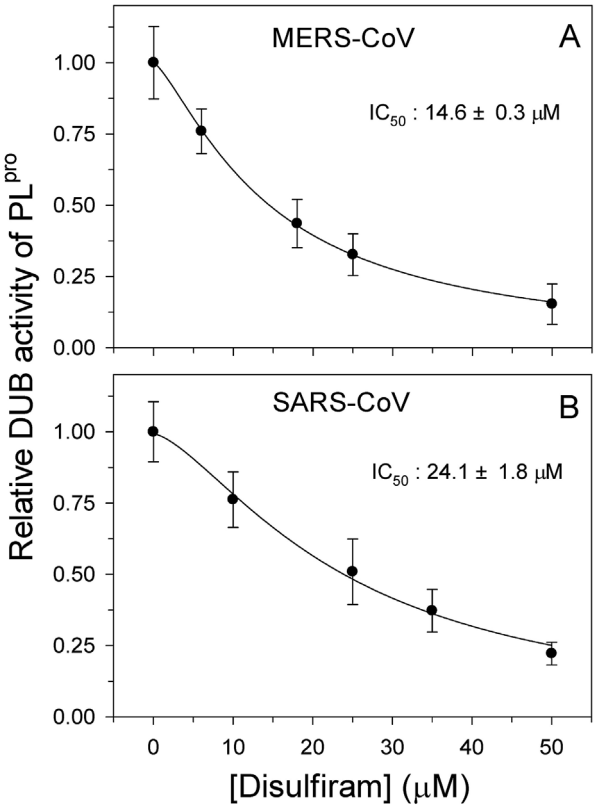

Fig. 1. Inhibitory effects of disulfiram on coronaviral PL^{pro}s. DUB activity of MERS-CoV (A) and SARS-CoV (B) PL^{pro} in the presence of disulfiram (6–50 μM) was measured. The concentration of fluorogenic substrate (Ub-AFC) was 0.25 μM, while the concentration of coronaviral PL^{pro} was 0.2 μM in both cases. The lines show best-fit results in accordance with the IC_{50} equation (Eq. (1)).

3. Results and discussion

3.1. The inhibition of MERS-CoV and SARS-CoV PL^{pro}s by disulfiram

PL^{pro}s are cysteine proteases that use the thiol group of cysteine as a nucleophile to attack the carbonyl group of the scissile peptide bond (Chou et al., 2014; Han et al., 2005; Verma et al., 2016). Inhibition can be expected if the catalytic cysteine of a PL^{pro} is interfered with or modified (Cheng et al., 2015; Chou et al., 2008). Disulfiram is known to be a thiol-reactive compound that can covalently modify cysteine residues (Diaz-Sanchez et al., 2016; Galkin et al., 2014; Lipsky et al., 2001; Paranjpe et al., 2014). To determine whether disulfiram can inhibit coronaviral PL^{pro}s, the DUB activity of MERS-CoV and SARS-CoV PL^{pro} was measured in the presence of various concentrations of disulfiram. Interestingly, disulfiram showed a dose-dependent inhibitory effect on both proteases with IC_{50} values in the micromolar range (Fig. 1). Next, to elucidate the kinetic mechanisms of the interactions between disulfiram and the two PL^{pro}s, the proteolytic activity of each enzyme was measured in the presence of various concentrations of a peptidyl substrate and disulfiram. The results were then fitted to different kinetic models (competitive, noncompetitive, uncompetitive and mixed inhibition). Surprisingly, disulfiram showed a noncompetitive inhibition pattern against MERS-CoV PL^{pro} (Fig. 2A) but a competitive inhibition pattern against SARS-CoV PL^{pro} (Fig. 2B). This inconsistency is quite intriguing since the two enzymes share a similar overall structure and an identical catalytic triad (Bailey-Elkin et al., 2014; Chou et al., 2014; Lei et al., 2014; Ratia et al., 2006), albeit the inhibition constant (K_{is}) of disulfiram for MERS-CoV PL^{pro} is 4.4-fold higher than that for SARS-CoV PL^{pro} (Table 1). Perhaps this discovery should not be surprising given that disulfiram is also a noncompetitive inhibitor for *Citrullus vulgaris* urease with a K_{is} of 67.6 μM (Diaz-Sanchez et al.,

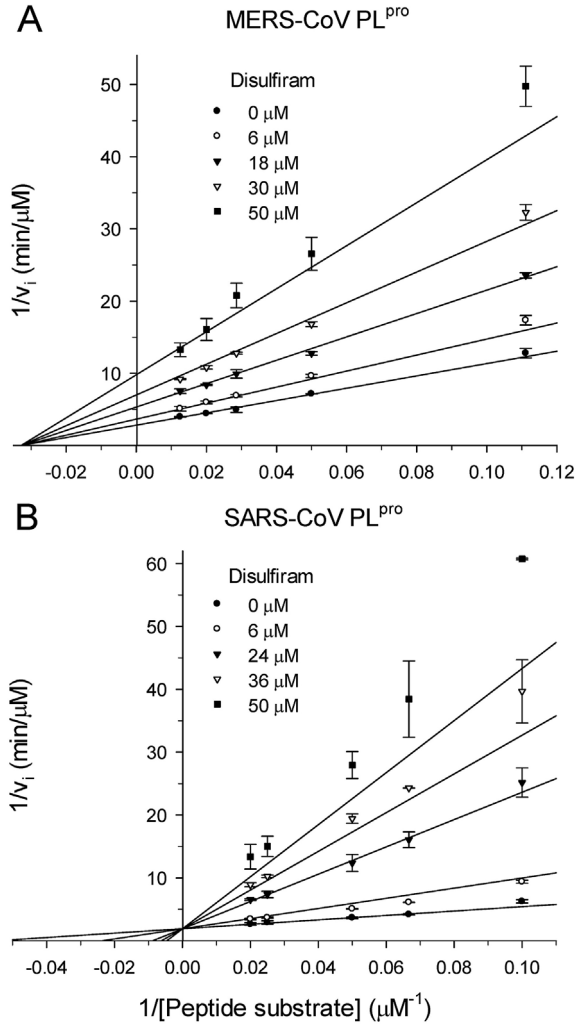

Fig. 2. Inhibition of coronaviral PL^{pro}s by disulfiram. The proteolytic activity of MERS-CoV (A) and SARS-CoV (B) PL^{pro} were measured in the presence of different peptide substrate concentrations (9–80 μM) and various concentrations of disulfiram (6–50 μM). The solid lines are best-fit results in accordance with noncompetitive (A) or competitive (B) inhibition models. The R_{sqr} values are 0.989 and 0.977, respectively. The experiments were repeated to ensure reproducibility. Kinetic parameters such as K_M, k_{cat} and K_{is} from the best-fit results are shown in Table 1.

2016), while its IC_{50} for *Giardia lamblia* carbamate kinase is 0.6–1.4 μM (Chen et al., 2012). Similarly, a previous study mentions that their compound 4 also has different recognition specificity for the two PL^{pro}s (Lee et al., 2015). Our study once again suggests broad-spectrum potency for disulfiram, given the versatility it shows even against two coronaviral PL^{pro}s.

3.2. Binding synergy analysis of coronaviral PL^{pro} inhibitors

The inconsistent inhibitory effect of disulfiram against the two PL^{pro}s suggests that the binding modes of disulfiram on the two enzymes may be different. To verify this, multiple inhibition assays using disulfiram and other known PL^{pro} inhibitors, including 6TG, MPA and NEM, were performed (Fig. 3) (Chen et al., 2009; Cheng et al., 2015; Yonetani and Theorell, 1964). Interestingly but not surprisingly, we found that disulfiram displays a synergistically inhibitory effect with either 6TG or MPA on MERS-CoV PL^{pro}, with the lines in the Yonetani-Theorell plots intersecting above the *x*-axis and α values below 1 in both cases (Fig. 3A and B) (Copeland, 2000). In contrast, in the case of SARS-CoV PL^{pro}, each of the plots displays two parallel lines and both α values are significantly higher than 1 (Fig. 3C and D), suggesting that binding of disulfiram and of 6TG or NEM are mutually exclusive on SARS-CoV PL^{pro} (Copeland, 2000). Since 6TG is a competitive inhibitor of both PL^{pro}s (Cheng et al., 2015; Chou et al., 2008), the contrasting synergy of disulfiram and 6TG on the two PL^{pro}s confirms the inconsistent inhibitory pattern of disulfiram (Figs. 2 and 3). Furthermore, MPA has previously been shown to be a noncompetitive inhibitor of MERS-CoV PL^{pro} and to work synergistically with 6TG to inhibit MERS-CoV PL^{pro} (Cheng et al., 2015). Combining those results with our results regarding the binding synergy of disulfiram and 6TG or MPA (Fig. 3A and B), we propose that disulfiram may occupy a third binding site on MERS-CoV PL^{pro}, neither a site at the active center nor the MPA binding site. Next, we evaluated PL^{pro} inhibition in the presence of disulfiram combined with 6TG and/or MPA by proteolytic assays using a peptidyl substrate. We found that the IC_{50} of disulfiram against MERS-CoV PL^{pro} showed a 1.6-fold decrease in the presence of 15 μM 6TG and a 5.2-fold decrease at 15 μM 6TG when it was tested in combination with 150 μM MPA (Table 2). For comparison, in the case of disulfiram against SARS-CoV PL^{pro}, there is no enhanced inhibitory effect in the presence of 6TG or NEM. Our results suggest a potential for using the above three FDA-approved drugs in combination treatments against MERS-CoV. Incidentally, previous studies have suggested that MPA may be used in combination treatments with interferon against MERS-CoV (Chan et al., 2013).

Table 1
Kinetic parameters of disulfiram inhibition of two coronaviral PL^{pro}s.

PL^{pro}/inhibitor	K_M (μM)	k_{cat} (s^{-1})	K_{is} (μM)	K_{inact} (μM)[c]	k_{max} ($10^{-2}s^{-1}$)[d]
SARS-CoV PL^{pro}					
No inhibitor	19.5 ± 4.9[a]	0.18 ± 0.03[a]			
Disulfiram				5.4 ± 0.3	1.1 ± 0.03
Competitive	18.3 ± 2.3[b]	0.17 ± 0.01[b]	4.6 ± 0.4[b]		
Mixed inhibition	19.5 ± 2.5[b]	0.18 ± 0.01[b]	6.0 ± 1.1[b]		
			43.8 ± 5.6[c]		
C271 mutant					
No inhibitor	24.6 ± 3.1[a]	0.12 ± 0.01[a]			
MERS-CoV PL^{pro}					
No inhibitor	28.8 ± 4.6[a]	0.01 ± 0.0004[a]			
Disulfiram	30.5 ± 1.8[b]	0.01 ± 0.0003[b]	20.1 ± 0.7[b]		

[a] The steady-state kinetic parameters of the PL^{pro}s were determined according to the Michaelis-Menten equation.
[b] In the presence of disulfiram, the best-fitted kinetic parameters and K_{is} were determined in accordance with competitive (Eq. (3)) or mixed inhibition (Eq. (4)) and noncompetitive (Eq. (2)) inhibition models for SARS-CoV and MERS-CoV PL^{pro}, respectively.
[c] The value is αK_{is}, the inhibition constant for the enzyme-substrate-inhibitor complex.
[d] K_{inact} and k_{max} values are from the best fit to the saturation equation (Eq. (7)).

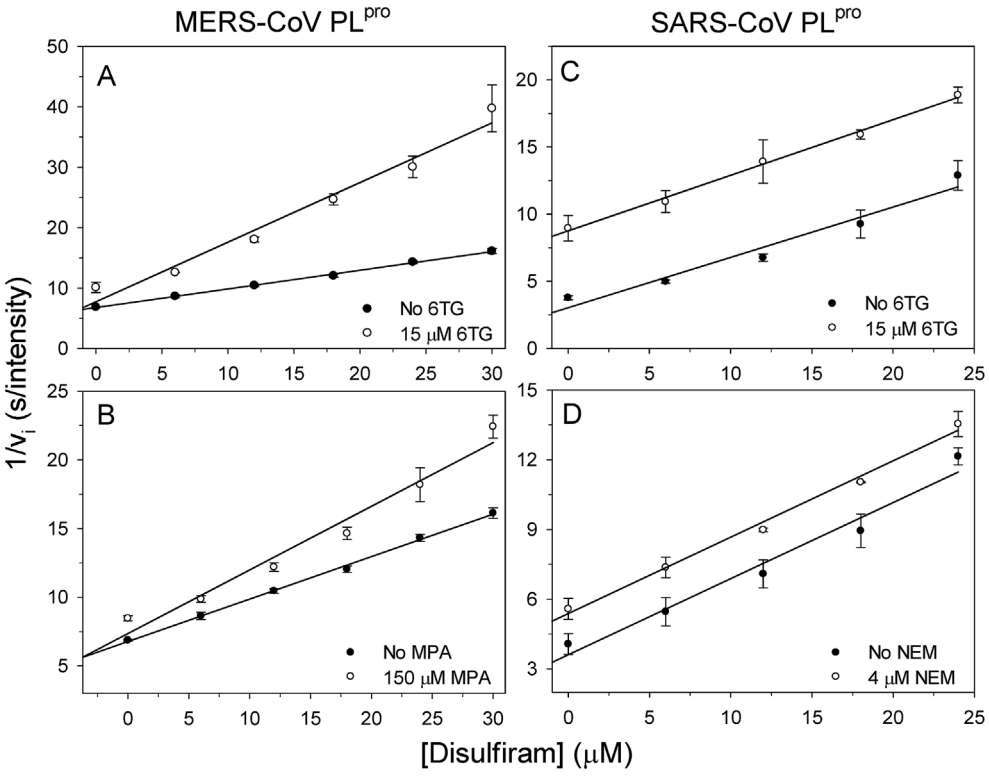

Fig. 3. Mutual effects of coronaviral PL^{pro} inhibitors. The activity of MERS-CoV PL^{pro} was measured without and with either 6TG (A) or MPA (B) in the presence of various concentrations of disulfiram, and that of SARS-CoV PL^{pro} was measured without and with either 6TG (C) or NEM (D) in the presence of various concentrations of disulfiram. The concentrations of peptidyl substrate and MERS-CoV PL^{pro} (A and B) were 20 and 0.6 μM, respectively, while those of peptidyl substrate and SARS-CoV PL^{pro} (C and D) were 15 and 0.05 μM, respectively. The points are the reciprocals of the initial velocities and the lines are the best fit of the data to Eq. (5). The results suggest that the α values for the four experiments (A–D) are 0.1, 0.17, 18.2 and 109.3, respectively.

Table 2
IC_{50} comparison of disulfiram inhibition of PL^{pro}s in the absence or presence of other inhibitors by proteolytic activity assay.

Enzyme	IC_{50} (μM)	IC_{50} fold decrement
SARS-CoV PL^{pro} inhibited by disulfiram	14.2 ± 0.5	–
with 6TG (15 μM)	21.8 ± 1.0	0.7
with NEM (4 μM)	18.1 ± 0.7	0.8
with βME (5 mM)	> 300	
SARS-CoV PL^{pro} C271A inhibited by disulfiram	62.7 ± 2.0	–
MERS-CoV PL^{pro} inhibited by disulfiram	22.7 ± 0.5[a,b,c]	–
with 6TG (15 μM)	14.5 ± 0.4[a]	1.6
with MPA (150 μM)	21.7 ± 0.4	1.0
with 6TG (10 μM) and MPA (100 μM)	13.7 ± 1.0[b]	1.7
with 6TG (15 μM) and MPA (150 μM)	4.4 ± 0.2[c]	5.2
with βME (5 mM)	> 300	

[a–c] $p < 0.05$ by Student's T test.

3.3. Disulfiram may also act as a zinc ejector

Previous studies suggested that disulfiram can bind to the zinc-bound cysteines in hepatitis C virus NS5A protein (Lee et al., 2016). As there are four cysteines bound to a zinc ion in PL^{pro}s (Fig. S2C and S2D) (Bailey-Elkin et al., 2014; Chou et al., 2014), we performed zinc ejection assays to test whether these zinc-bound cysteines may be a candidate for the aforementioned "third binding site" occupied by disulfiram on MERS-CoV PL^{pro}. In the present study, the zinc-specific fluorophore, FluoZin-3, was used to identify the release of zinc ion due to the binding of disulfiram to the enzyme (Fig. 4A). Unexpectedly, we

Table 3
X-ray diffraction data collection and refinement statistics.

	SARS-CoV PL^{pro}-βME complex	SARS-CoV PL^{pro}-glycerol complex
Data collection		
Space group	C2	C2
Cell dimensions		
a, *b*, *c* (Å)	151.4, 33.3, 90.7	151.2, 33.4, 90.9
α, β, γ (°)	90, 125, 90	90, 125, 90
Resolution[a] (Å)	30–1.65 (1.71–1.65)	30–1.65 (1.71–1.65)
R_{merge}[b] (%)	4.1 (34.7)	4.7 (45.6)
$I/\sigma I$	29.0 (3.6)	26.3 (3.6)
Completeness (%)	99.7 (98.2)	95.5 (94.8)
Redundancy	3.6 (3.6)	3.5 (3.7)
Refinement		
Number of reflections	42,759 (6082)	41,221 (5917)
R factor[c] (%)	14.7 (16.3)	16.2 (17.7)
Free *R* factor[d] (%)	18.4 (20.1)	19.9 (21.7)
Number of atoms	2994	2899
Protein	2676	2659
Ligand/ion	16/6	18/6
Water	298	216
B-factors (Å^2)		
Protein	16.5	27.8
Ligand/ion	27.0/21.3	34.5/31.8
Water	28.2	34.8
rmsd		
Bond length (Å)	0.007	0.008
Bond angles (°)	1.3	1.3
Ramachandran analysis (%)		
Favored	92.3	93.0
Allowed	7.7	7.0

[a] The numbers in parentheses are for the highest-resolution shell.

[b] $R_{merge} = \sum_h \sum_i |I_{hi} - \langle I_h \rangle| / \sum_h \sum_i I_{hi}$, where I_{hi} is the integrated intensity of a given reflection and $\langle I_h \rangle$ is the mean intensity of multiple corresponding symmetry-related reflections.

[c] $R = \sum_h |F_h^o - F_h^c| / \sum_h F_h^o$, where F_h^o and F_h^c are the observed and calculated structure factors, respectively.

[d] Free *R* is *R* calculated using a random 5% of data excluded from the refinement.

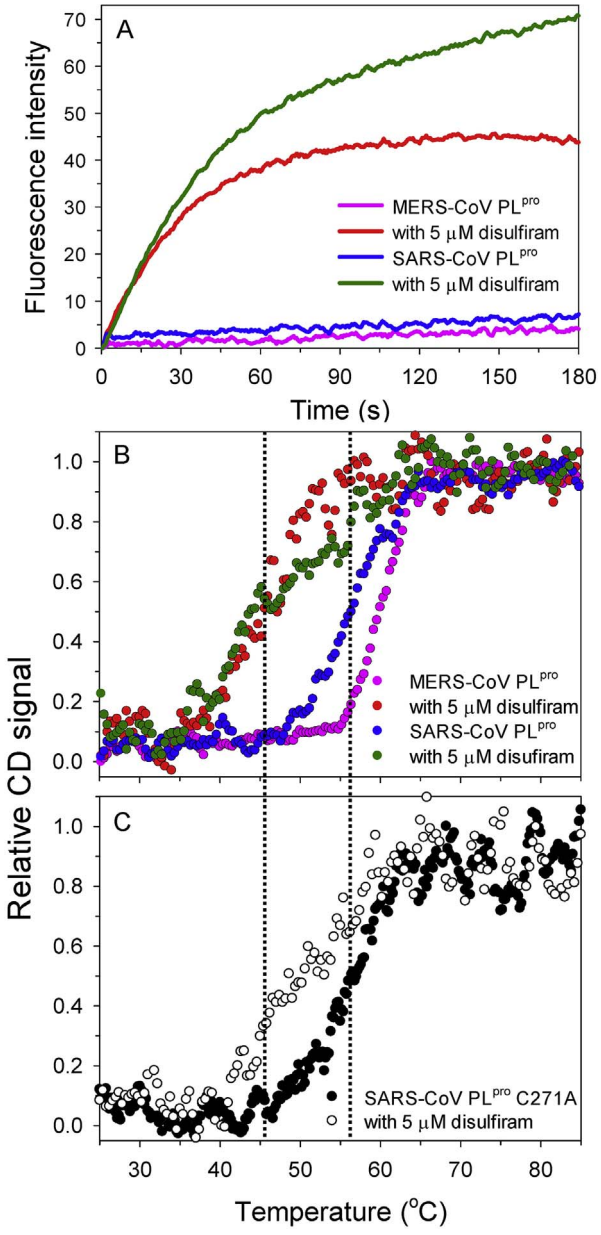

Fig. 4. Effect of zinc ion ejection by disulfiram and its influence on PL^{pro} stability. (A) MERS- and SARS-CoV PL^{pro} each was incubated without and with 5 μM disulfiram. The release of zinc ions from the enzyme was detected as the increase of the fluorescence signal of the zinc-specific fluorophore FluoZin-3. (B) and (C) Thermostability of MERS-CoV PL^{pro}, SARS-CoV PL^{pro} or SARS-CoV PL^{pro} C271A mutant in the absence or presence of 5 μM disulfiram was detected by circular dichroism spectrometry. The protein concentration was 0.2 mg/ml. The wavelength used was 222 nm and the cuvette pathlength was 1 mm. The right and left dotted lines show the melting temperature of SARS-CoV PL^{pro} without and with disulfiram, respectively. These results indicate that disulfiram destabilized the enzyme.

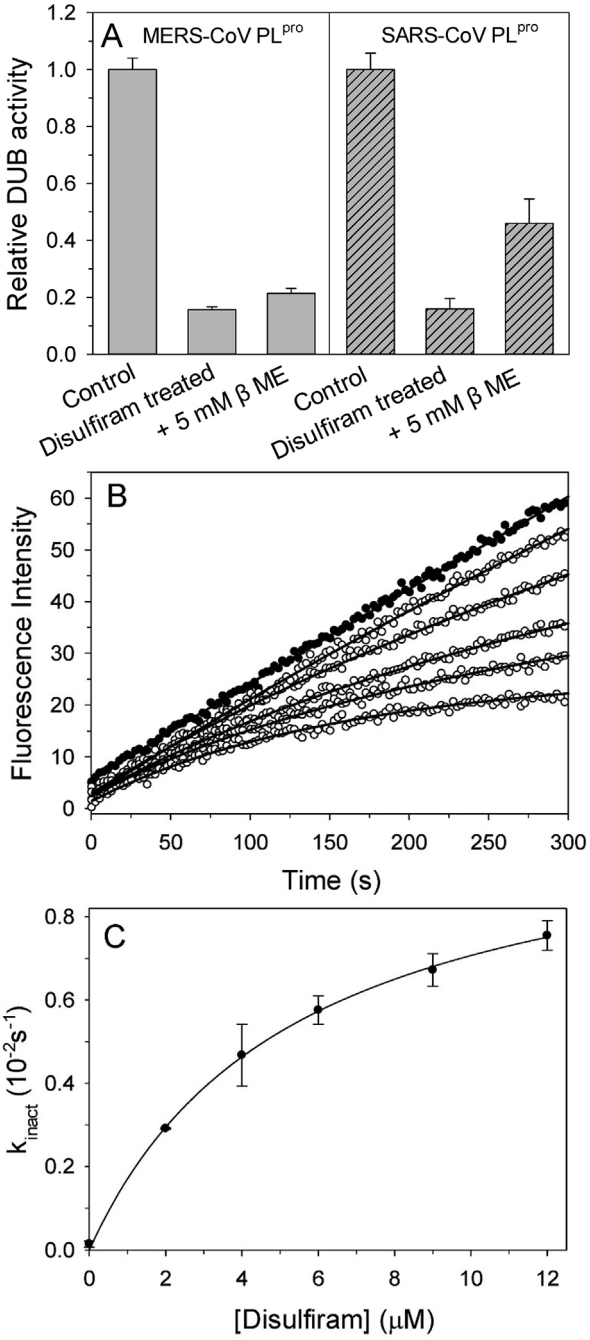

Fig. 5. Slow-binding inhibition of SARS-CoV PL^{pro} by disulfiram. (A) DUB activity of disulfiram-treated MERS- and SARS-CoV PL^{pro} in the absence or presence of 5 mM β-ME. The enzyme was incubated without or with 200 μM disulfiram for 1 h and the mixture was then desalted using a Sephadex G-25 column. The concentrations of fluorogenic substrate (Ub-AFC) and enzyme were 0.25 and 0.2 μM, respectively. (B) 0.05 μM SARS-CoV PL^{pro} was incubated with different concentrations of disulfiram (0 μM, closed circles; 2–12 μM, open circles), after which its proteolytic activity was measured for 5 min using 15 μM peptidyl substrate. The solid lines are best-fit results in accordance with the slow-binding equation (Eq. (6)). (C) The observed inactivation rate constants (k_{inact}) from panel B were replotted against disulfiram concentration. The solid line is the best-fit result in accordance with the saturation equation (Eq. (7)). Kinetic parameters K_{inact} and k_{max} corresponding to the best-fit curve are shown in Table 1.

observed significant zinc release in the presence of disulfiram not only from MERS-CoV PL^{pro} but also from SARS-CoV PL^{pro}. This result indicates that disulfiram may bind not only to the active site but also to the zinc-binding sites in SARS-CoV PL^{pro}. Following this finding, we tried to fit our inhibitory results to a mixed inhibition model (Fig. S1). The two K_{is} for the enzyme-substrate and enzyme-substrate-inhibitor complexes were 6.0 and 43.8 μM, respectively, showing a 7.3-fold difference in the binding affinity for the two putative binding sites (Table 1). This significant difference may explain why the inhibitory pattern of disulfiram against SARS-CoV PL^{pro} looks more like competitive inhibition. Next, the thermostability of the two PL^{pro}s in the absence and presence of disulfiram was evaluated (Fig. 4B). Not surprisingly, the melting temperature of both PL^{pro}s decreased 10–15 °C in the presence of disulfiram. These results conform to our earlier finding that the release of zinc ion can destabilize PL^{pro} (Chou et al., 2012).

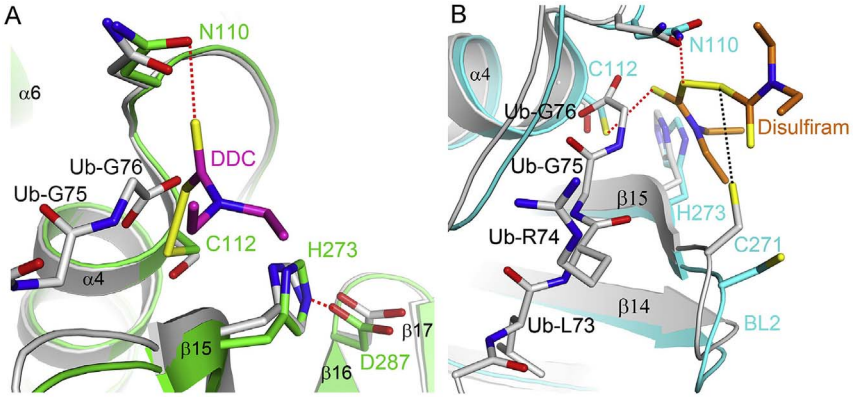

Fig. 6. Binding of disulfiram to SARS-CoV PL^{pro}. Overlay of model structure of SARS-CoV PL^{pro} in complex with DDC (magenta) (A) or disulfiram (orange) (B) with the crystal structure of SARS-CoV PL^{pro} in complex with ubiquitin (gray, PDB code: 4M0W). DDC and disulfiram are modeled based on the binding sites of βME and glycerol, respectively. The red dashed lines show putative polar interactions while the black dashed line shows the distance between residue Cys271 and disulfiram as 4.0 Å. (For interpretation of the references to colour in this figure legend, the reader is referred to the web version of this article.)

3.4. Time-dependent inhibition of SARS-CoV PL^{pro} by disulfiram

Disulfiram is known to covalently modify cysteine residues and leave a diethyldithiolcarbamate (DDC) moiety to inactivate the carbamate kinase of *Giardia lamblia* (Galkin et al., 2014). In the presence of 5 mM βME, however, the inhibitory effect of disulfiram against PL^{pro}s is minor and the IC_{50} is larger than 300 μM (Table 2). This suggests that the reductant can protect the enzyme and, therefore, that disulfiram may inhibit the enzyme by modifying the cysteine in the catalytic triad (Cys112-His273-Asp287). To further investigate this possibility, the DUB activity of the enzyme was measured after incubation with 200 μM disulfiram for 1 h followed by removal of the small molecules using a Sephadex G-25 column. This treatment resulted in an 84% loss of activity, suggesting irreversible inhibition of SARS-CoV PL^{pro} by disulfiram (Fig. 5A, right panel). Similarly, in a previous *in vivo* study, disulfiram-treated aldehyde dehydrogenase showed 77% enzyme inhibition as compared to the activity of the control (Lipsky et al., 2001). Next, the disulfiram-treated SARS-CoV PL^{pro} was incubated with 5 mM βME for 10 min, after which activity was measured to test for re-activation. We found that 30% of the enzyme's activity was restored after treatment with βME (Fig. 5A, right panel). The rescuing effect of the reductant suggests that the modification was due to the disulfide bonding interaction between the enzyme and the inhibitor. However, in the case of MERS-CoV PL^{pro}, we found that treatment with disulfiram resulted in an irreversible loss of activity which was not rescued by the addition of the reductant (Fig. 5A, left panel). Previous studies have suggested that the release of zinc ion following treatment with EDTA will lead to a 62% loss of PL^{pro} activity (Chou et al., 2012). This result is consistent with the effect of disulfiram on PL^{pro}s. Also, the inability of the reductant to rescue the DUB activity of MERS-CoV PL^{pro}, suggesting that disulfiram cannot influence its active site, is compatible with disulfiram's noncompetitive mode of inhibition of the enzyme.

On the other hand, proteolytic assays of SARS-CoV PL^{pro} at various concentrations of disulfiram showed dose- and time-dependent decay when enzyme activity was measured for 5 min (Fig. 5B). By fitting the data to Eq. (6), different k_{inact} values at various concentrations of disulfiram were determined and then plotted versus those disulfiram concentrations (Fig. 5C). The saturated curvature suggests a slow-binding phenomenon due to covalent inactivation (Copeland, 2000), a conclusion supported by the irrecoverability of enzyme activity after disulfiram removed (Fig. 5A). Best-fit analysis determined a K_{inact} of 5.4 μM and a k_{max} of 0.011 s^{-1} (Fig. 5C and Table 1). Interestingly, the K_{inact} value is close to K_{is}, indicating that disulfiram may inactivate the enzyme very soon after binding. For comparison, previous studies have indicated that 6-mercaptopurine and 6TG are also slow-binding inhibitors against the same enzyme, albeit enzyme activity was recovered after removing the inhibitors (Chou et al., 2008).

3.5. Proposed binding mechanism of disulfiram to SARS-CoV and MERS-CoV PL^{pro}s

The structure of SARS-CoV PL^{pro} in complex with disulfiram should allow us to understand the binding mechanism more clearly. Accordingly, we attempted to crystallize SARS-CoV PL^{pro} in the presence of disulfiram. Unfortunately, although crystals of the protein were formed in the presence of 0.4 mM disulfiram, the crystal structure showed only βME-like electron density near the active-site cysteine with no omit electron density shown near the zinc-binding site (Fig. S2A and S2C). βME is a reducing agent that is added into the purification buffer to stabilize the protein, and which is also known to reverse the effect of disulfiram (Table 2, Fig. 5A and Kitson, 1975). To avoid this effect, we eliminated all reducing agents from the purification process, added 50 μM disulfiram into all purification buffers, and then attempted to crystallize the protein purified under these conditions. Although we were able to grow crystals under different crystallization conditions, we again obtained an unexpected result, as the only omit electron density near the catalytic site was fitted as a glycerol molecule (Fig. S2B and S2D). This result might be due to the crystals having been cryoprotected in reservoir solution supplemented with 25% (v/v) glycerol. Nevertheless, the binding of βME and glycerol near the active site suggests that the active site may be accessible to disulfiram. Next, using the aforementioned two complex structures, a disulfiram and a DDC molecule were docked into the glycerol and βME binding sites, respectively (Fig. 6). DDC may be able to covalently bind to residue Cys112 in a manner similar to that of βME (Fig. 6A), while disulfiram may be able to occupy the glycerol site (Fig. 6B). Interestingly, in the docking structure of the PL^{pro}-disulfiram complex, we can see that one sulfur atom of the disulfide bond of disulfiram is within 4 Å of residue Cys271 at blocking loop 2 (BL2), which is very important for substrate and inhibitor binding (Chou et al., 2014; Ratia et al., 2008). For comparison, there is a valine at the same site in MERS-CoV PL^{pro} (Bailey-Elkin et al., 2014; Chou et al., 2014). To verify the possible inhibitory effect of disulfiram due to binding to residue Cys271, inhibition of the SARS-CoV PL^{pro} C271A mutant by disulfiram was measured (Fig. S3). Interestingly, we can see a 4.4-fold increase in IC_{50} (Table 2) compared with that for inhibition of wild-type SARS-CoV PL^{pro} by disulfiram. In addition, the decrease of the melting temperature of the C271A mutant following treatment with disulfiram is 6 °C, lower than that of wild-type SARS-CoV PL^{pro} treatment with the same inhibitor (Fig. 4B and C). These findings suggest that disulfiram may inhibit SARS-CoV PL^{pro} partly via the residue Cys271 and support the reliability of the docking of disulfiram on the glycerol binding site. Based on our kinetic and structural results, we propose kinetic mechanism schemes for the inhibition of the two PL^{pro}s by disulfiram (Fig. 7). Similar to the mechanism in the case of disulfiram-treated urease (Diaz-Sanchez et al., 2016), disulfiram may form a covalent adduct with SARS-CoV PL^{pro} and then leave a DDC on the active-site Cys112, preventing downstream acylation and thereby inactivating the

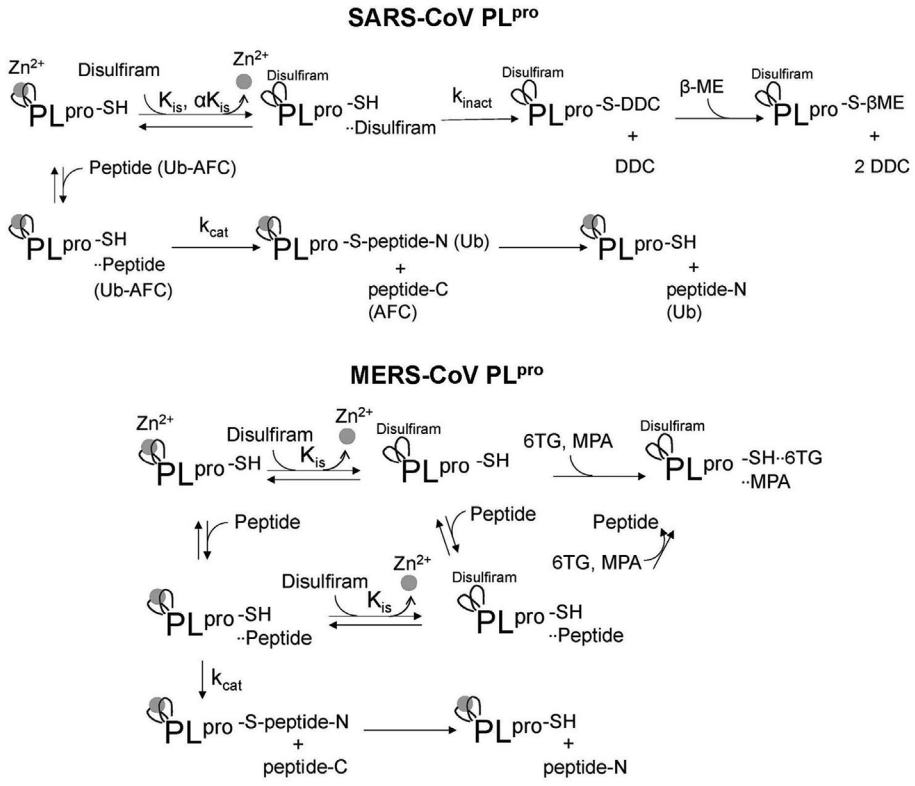

Fig. 7. Schemes of proposed kinetic mechanisms for the inhibition of SARS-CoV and MERS-CoV PL^{pro} by disulfiram. The upper diagram denotes enzyme catalysis, mixed inhibition and inactivation of SARS-CoV PL^{pro} by disulfiram. The lower diagram shows noncompetitive inhibition of MERS-CoV PL^{pro} by disulfiram and triple inhibition with two other FDA-approved drugs, 6TG and MPA. SH symbolizes the thiolate of catalytic triad residue Cys.

enzyme. In contrast, disulfiram shows a noncompetitive inhibitory effect against MERS-CoV PL^{pro} and can synergistically inhibit that enzyme with 6TG and MPA.

4. Conclusion

In this study, we found that disulfiram is, respectively, a noncompetitive and competitive (or mixed) inhibitor of MERS-CoV and SARS-CoV PL^{pro}s. Multiple inhibition assays also support a kinetic mechanism by which disulfiram together with 6TG and/or MPA can synergistically inhibit MERS-CoV PL^{pro}, but not, due to its competitive mode of inhibition, SARS-CoV PL^{pro}. On the other hand, the results of kinetic assays, continued inactivation after the removal of disulfiram, reactivation by reductant, and the phenomenon of slow-binding inhibition suggest that disulfiram may act at the active site of SARS-CoV PL^{pro}, forming a covalent adduct with residue Cys112. Crystal structures of the enzyme in complex with glycerol and βME imply that the active site is solvent-exposed and accessible for disulfiram or DDC binding.

Acknowledgements

We would like to thank Ziad Omran for helpful suggestions. This research was supported by grants from the Ministry of Science and Technology, Taiwan, ROC (104-2320-B-010-034, 105-2320-B-010-012 and 106-2320-B-010-013) to CYC and a CGMH-NYMU joint research grant (CMRPG2F0431) to CYS and CYC. We are grateful for the experimental facilities and the technical services provided by the Synchrotron Radiation Protein Crystallography Facility, which is supported by the National Core Facility Program for Biotechnology, Ministry of Science and Technology, Taiwan, ROC, and the National Synchrotron Radiation Research Center, a national user facility supported by the Ministry of Science and Technology, Taiwan, ROC.

Appendix A. Supplementary data

Supplementary data related to this article can be found at http://dx.doi.org/10.1016/j.antiviral.2017.12.015.

References

Bailey-Elkin, B.A., Knaap, R.C., Johnson, G.G., Dalebout, T.J., Ninaber, D.K., van Kasteren, P.B., Bredenbeek, P.J., Snijder, E.J., Kikkert, M., Mark, B.L., 2014. Crystal structure of the Middle East respiratory syndrome coronavirus (MERS-CoV) papain-like protease bound to ubiquitin facilitates targeted disruption of deubiquitinating activity to demonstrate its role in innate immune suppression. J. Biol. Chem. 289, 34667–34682.

Bell, R.G., Smith, H.W., 1949. Preliminary report on clinical trials of antabuse. Can. Med. Assoc. J. 60, 286–288.

Chan, J.F., Chan, K.H., Kao, R.Y., To, K.K., Zheng, B.J., Li, C.P., Li, P.T., Dai, J., Mok, F.K., Chen, H., Hayden, F.G., Yuen, K.Y., 2013. Broad-spectrum antivirals for the emerging Middle East respiratory syndrome coronavirus. J. Infect. 67, 606–616.

Chen, C.Z., Southall, N., Galkin, A., Lim, K., Marugan, J.J., Kulakova, L., Shinn, P., van Leer, D., Zheng, W., Herzberg, O., 2012. A homogenous luminescence assay reveals novel inhibitors for giardia lamblia carbamate kinase. Curr. Chem. Genomics 6, 93–102.

Chen, X., Chou, C.Y., Chang, G.G., 2009. Thiopurine analogue inhibitors of severe acute respiratory syndrome-coronavirus papain-like protease, a deubiquitinating and deISGylating enzyme. Antivir. Chem. Chemother. 19, 151–156.

Cheng, K.W., Cheng, S.C., Chen, W.Y., Lin, M.H., Chuang, S.J., Cheng, I.H., Sun, C.Y., Chou, C.Y., 2015. Thiopurine analogs and mycophenolic acid synergistically inhibit the papain-like protease of Middle East respiratory syndrome coronavirus. Antiviral Res. 115, 9–16.

Chou, C.Y., Chien, C.H., Han, Y.S., Prebanda, M.T., Hsieh, H.P., Turk, B., Chang, G.G., Chen, X., 2008. Thiopurine analogues inhibit papain-like protease of severe acute respiratory syndrome coronavirus. Biochem. Pharmacol. 75, 1601–1609.

Chou, C.Y., Lai, H.Y., Chen, H.Y., Cheng, S.C., Cheng, K.W., Chou, Y.W., 2014. Structural basis for catalysis and ubiquitin recognition by the severe acute respiratory syndrome coronavirus papain-like protease. Acta Crystallogr. Sect. D Biol. Crystallogr. 70, 572–581.

Chou, Y.W., Cheng, S.C., Lai, H.Y., Chou, C.Y., 2012. Differential domain structure stability of the severe acute respiratory syndrome coronavirus papain-like protease. Arch. Biochem. Biophys. 520, 74–80.

Clementz, M.A., Chen, Z., Banach, B.S., Wang, Y., Sun, L., Ratia, K., Baez-Santos, Y.M., Wang, J., Takayama, J., Ghosh, A.K., Li, K., Mesecar, A.D., Baker, S.C., 2010. Deubiquitinating and interferon antagonism activities of coronavirus papain-like proteases. J. Virol. 84, 4619–4629.

Copeland, R., 2000. Enzymes: a Practical Introduction to Structure, Mechanism, and Data

Analysis. Wiley-VCH Inc.
Diaz-Sanchez, A.G., Alvarez-Parrilla, E., Martinez-Martinez, A., Aguirre-Reyes, L., Orozpe-Olvera, J.A., Ramos-Soto, M.A., Nunez-Gastelum, J.A., Alvarado-Tenorio, B., de la Rosa, L.A., 2016. Inhibition of urease by disulfiram, an FDA-approved thiol reagent used in humans. Molecules 21.
Elliott, J.H., McMahon, J.H., Chang, C.C., Lee, S.A., Hartogensis, W., Bumpus, N., Savic, R., Roney, J., Hoh, R., Solomon, A., Piatak, M., Gorelick, R.J., Lifson, J., Bacchetti, P., Deeks, S.G., Lewin, S.R., 2015. Short-term administration of disulfiram for reversal of latent HIV infection: a phase 2 dose-escalation study. Lancet HIV 2, e520–529.
Emsley, P., Cowtan, K., 2004. Coot: model-building tools for molecular graphics. Acta Crystallogr. Sect. D Biol. Crystallogr. 60, 2126–2132.
Frieman, M., Ratia, K., Johnston, R.E., Mesecar, A.D., Baric, R.S., 2009. Severe acute respiratory syndrome coronavirus papain-like protease ubiquitin-like domain and catalytic domain regulate antagonism of IRF3 and NF-kappaB signaling. J. Virol. 83, 6689–6705.
Galkin, A., Kulakova, L., Lim, K., Chen, C.Z., Zheng, W., Turko, I.V., Herzberg, O., 2014. Structural basis for inactivation of Giardia lamblia carbamate kinase by disulfiram. J. Biol. Chem. 289, 10502–10509.
Han, Y.S., Chang, G.G., Juo, C.G., Lee, H.J., Yeh, S.H., Hsu, J.T., Chen, X., 2005. Papain-like protease 2 (PLP2) from severe acute respiratory syndrome coronavirus (SARS-CoV): expression, purification, characterization, and inhibition. Biochemistry 44, 10349–10359.
Hilgenfeld, R., Peiris, M., 2013. From SARS to MERS: 10 years of research on highly pathogenic human coronaviruses. Antiviral Res. 100, 286–295.
Kitson, T.M., 1975. The effect of disulfiram on the aldehyde dehydrogenases of sheep liver. Biochem. J. 151, 407–412.
Krampe, H., Ehrenreich, H., 2010. Supervised disulfiram as adjunct to psychotherapy in alcoholism treatment. Curr. Pharm. Des. 16, 2076–2090.
Lee, H., Lei, H., Santarsiero, B.D., Gatuz, J.L., Cao, S., Rice, A.J., Patel, K., Szypulinski, M.Z., Ojeda, I., Ghosh, A.K., Johnson, M.E., 2015. Inhibitor recognition specificity of MERS-CoV papain-like protease may differ from that of SARS-CoV. ACS Chem. Biol. 10, 1456–1465.
Lee, Y.M., Duh, Y., Wang, S.T., Lai, M.M., Yuan, H.S., Lim, C., 2016. Using an old drug to target a new drug site: application of disulfiram to target the Zn-Site in HCV NS5A protein. J. Am. Chem. Soc. 138, 3856–3862.
Lei, J., Mesters, J.R., Drosten, C., Anemuller, S., Ma, Q., Hilgenfeld, R., 2014. Crystal structure of the papain-like protease of MERS coronavirus reveals unusual, potentially druggable active-site features. Antiviral Res. 109, 72–82.
Lin, M.H., Chuang, S.J., Chen, C.C., Cheng, S.C., Cheng, K.W., Lin, C.H., Sun, C.Y., Chou, C.Y., 2014. Structural and functional characterization of MERS coronavirus papain-like protease. J. Biomed. Sci. 21, 54.
Lipsky, J.J., Shen, M.L., Naylor, S., 2001. In vivo inhibition of aldehyde dehydrogenase by disulfiram. Chem. Biol. Interact. 130–132, 93–102.
McCoy, A.J., Grosse-Kunstleve, R.W., Adams, P.D., Winn, M.D., Storoni, L.C., Read, R.J., 2007. Phaser crystallographic software. J. Appl. Crystallogr. 40, 658–674.
Menachery, V.D., Yount Jr., B.L., Debbink, K., Agnihothram, S., Gralinski, L.E., Plante, J.A., Graham, R.L., Scobey, T., Ge, X.Y., Donaldson, E.F., Randell, S.H., Lanzavecchia, A., Marasco, W.A., Shi, Z.L., Baric, R.S., 2015. A SARS-like cluster of circulating bat coronaviruses shows potential for human emergence. Nat. Med. 21, 1508–1513.
Menachery, V.D., Yount Jr., B.L., Sims, A.C., Debbink, K., Agnihothram, S.S., Gralinski, L.E., Graham, R.L., Scobey, T., Plante, J.A., Royal, S.R., Swanstrom, J., Sheahan, T.P., Pickles, R.J., Corti, D., Randell, S.H., Lanzavecchia, A., Marasco, W.A., Baric, R.S., 2016. SARS-like WIV1-CoV poised for human emergence. Proc. Natl. Acad. Sci. U. S. A. 113, 3048–3053.
Moore, S.A., Baker, H.M., Blythe, T.J., Kitson, K.E., Kitson, T.M., Baker, E.N., 1998. Sheep liver cytosolic aldehyde dehydrogenase: the structure reveals the basis for the retinal specificity of class 1 aldehyde dehydrogenases. Structure 6, 1541–1551.
Murshudov, G.N., Skubak, P., Lebedev, A.A., Pannu, N.S., Steiner, R.A., Nicholls, R.A., Winn, M.D., Long, F., Vagin, A.A., 2011. REFMAC5 for the refinement of macromolecular crystal structures. Acta Crystallogr. Sect. D Biol. Crystallogr. 67, 355–367.
Otwinowski, Z., Minor, W., 1997. Processing of X-ray diffraction data collected in oscillation mode. Methods Enzymol. 276, 307–326.
Paranjpe, A., Zhang, R., Ali-Osman, F., Bobustuc, G.C., Srivenugopal, K.S., 2014. Disulfiram is a direct and potent inhibitor of human O6-methylguanine-DNA methyltransferase (MGMT) in brain tumor cells and mouse brain and markedly increases the alkylating DNA damage. Carcinogenesis 35, 692–702.
Perlman, S., Netland, J., 2009. Coronaviruses post-SARS: update on replication and pathogenesis. Nat. Rev. Microbiol. 7, 439–450.
Ratia, K., Pegan, S., Takayama, J., Sleeman, K., Coughlin, M., Baliji, S., Chaudhuri, R., Fu, W., Prabhakar, B.S., Johnson, M.E., Baker, S.C., Ghosh, A.K., Mesecar, A.D., 2008. A noncovalent class of papain-like protease/deubiquitinase inhibitors blocks SARS virus replication. Proc. Natl. Acad. Sci. U. S. A. 105, 16119–16124.
Ratia, K., Saikatendu, K.S., Santarsiero, B.D., Barretto, N., Baker, S.C., Stevens, R.C., Mesecar, A.D., 2006. Severe acute respiratory syndrome coronavirus papain-like protease: structure of a viral deubiquitinating enzyme. Proc. Natl. Acad. Sci. U. S. A. 103, 5717–5722.
Verma, S., Dixit, R., Pandey, K.C., 2016. Cysteine proteases: modes of activation and future prospects as pharmacological targets. Front. Pharmacol. 7, 107.
Yang, X., Chen, X., Bian, G., Tu, J., Xing, Y., Wang, Y., Chen, Z., 2014. Proteolytic processing, deubiquitinase and interferon antagonist activities of Middle East respiratory syndrome coronavirus papain-like protease. J. Gen. Virol. 95, 614–626.
Yonetani, T., Theorell, H., 1964. Studies on liver alcohol hydrogenase complexes. 3. Multiple inhibition kinetics in the presence of two competitive inhibitors. Arch. Biochem. Biophys. 106, 243–251.
Zaki, A.M., van Boheemen, S., Bestebroer, T.M., Osterhaus, A.D., Fouchier, R.A., 2012. Isolation of a novel coronavirus from a man with pneumonia in Saudi Arabia. N. Engl. J. Med. 367, 1814–1820.
Zheng, D., Chen, G., Guo, B., Cheng, G., Tang, H., 2008. PLP2, a potent deubiquitinase from murine hepatitis virus, strongly inhibits cellular type I interferon production. Cell Res. 18, 1105–1113.